# Chemo-, Regio-, and Stereoselective Assembly of Polysubstituted Furan-2(5*H*)-ones Enabled by Rh(III)-Catalyzed Domino C–H Alkenylation/DG Migration/Lactonization: A Combined Experimental and Computational Study

Fei Zhao,[†,#,*] Zhi Zhou,[⊥,#] Yangbin Lu,[†,#] Jin Qiao,[†] Xiaoning Zhang,[†] Xin Gong,[†] Siyu Liu,[†] Shuang Lin,[⊥] Xiaowei Wu,[§,∥,*] and Wei Yi[⊥,*]

[†] Antibiotics Research and Re-evaluation Key Laboratory of Sichuan Province, Sichuan Industrial Institute of Antibiotics, School of Pharmacy, Chengdu University, Chengdu 610106, China.

[⊥] Key Laboratory of Molecular Target and Clinical Pharmacology & State Key Laboratory of Respiratory Disease, School of Pharmaceutical Sciences & the Fifth Affiliated Hospital, Guangzhou Medical University, Guangzhou, Guangdong 511436, China.

[§] Shanghai Institute of Materia Medica, Chinese Academy of Sciences, Shanghai 201203, China.

[∥] Zhongshan Institute for Drug Discovery, Shanghai Institute of Materia Medica, Chinese Academy of Sciences, Zhongshan 528400, China.

KEYWORDS: *rhodium(III) catalysis, C–H activation, domino reaction, furan-2(5H)-ones, 5-hydroxyfuran-2(5H)-ones, DFT calculations*

ABSTRACT: Exploring multi-step cascade reactions triggered by C−H activation are recognized as appealing, yet challenging. Herein, we disclose a Rh(III)-catalyzed domino C–H coupling of *N*-carbamoyl indoles and 4-hydroxy-2-alkynoates for the streamlined assembly of highly

functionalized furan-2(5*H*)-ones, in which the carbamoyl directing group is given a dual role of auxiliary group and migrating acylating reagent via the cleavage of the stable C−N bond at room temperature. More importantly, the obtained furan-2(5*H*)-one skeleton could be further functionalized under air in situ via C5–H hydroxylation by simply switching the solvent or additive, providing the fully substituted furan-2(5*H*)-ones with the installation of an alcohol-based $C_5$ quaternary carbon center. Detailed experimental studies and DFT calculations reveal that a Rh(III)-mediated tandem C–H activation/alkyne insertion/DG migration/lactonization accounts for the developed transformation to achieve the high functionalities with the observed exclusive selectivity. The potential biological application of the obtained furan-2(5*H*)-ones as a class of potent PPARγ ligands further highlights the synthetic utility of the developed methodology. This protocol is endowed with several salient features including efficient multi-step cascade triggered by C−H activation, excellent chemo-, regio- and stereoselectivity, high bond-forming efficiency (*e.g.*, two C−C and two C−O bonds), solvent- or additive-controlled product selectivity, good functional group compatibility and mild redox-neutral conditions.

## INTRODUCTION

Over the past two decades, transition-metal (TM)-catalyzed C−H functionalization with the assistance of heteroatom-based monodentate and bidentate directing groups (DGs) has emerged as one of effective approaches for the synthesis of a variety of structurally diverse molecules due to its high efficiency in carbon–carbon/heteroatom bond construction without the prefunctionalization of starting materials.[1] In principle, DG chelation-assisted *ortho*-metalation occurs at first in C−H functionalization to produce an active nucleophilic metallacycle intermediate, which then adds to various coupling partners (CPs) to afford the functionalized

products (Scheme 1a).[2] Therefore, DGs are initially designed and employed as auxiliary groups, which help to improve regioselectivity as well as reactivity, and in most case simply remain at their original locations when reactions finish or in some case undergo further intramolecular cyclization in situ.[3] However, in this context, a nonnegligible fact is that the chemical traces of DGs might not be wanted in the products and impede downstream transformations, and tedious steps are often required to remove them because DGs are usually tethered to the substrates via stable C−C/N/O bonds, thus resulting in unsatisfactory step- and atom-economy. In addition, a stoichiometric amount of external oxidants is also mandatorily required for the turnover of the catalytic cycle because of the oxidative character of these C−H activation reactions.

To overcome the abovementioned shortcomings, one recently emerging strategy of employing traceless oxidizing DGs containing readily broken N−O, N−N or O−O bonds, which could be easily auto-cleaved in situ during the reaction, in a sense could address the issue of DG removal and enable the related reactions with a redox-neutral feature. But it still suffers from unsatisfactory atom-economy as water, alcohol, amide, or carboxylic acid are produced as by-products,[4] even though recently several breakthroughs involving the intramolecular migration of the broken fragment from the cleavage of N−O, N−N or O−O bonds have been made[5] through the relatively complicated modification of the coordination environment and saturation of the TM center.[6] Evidently, it is quite fascinating but also challenging to achieve the DG-mediated redox-neutral C−H activation and subsequent migration cascade to meet the concept of "green and sustainable" C−H functionalization (Scheme 1b),[6a-e,7-12] especially via the formal cleavage of more stable chemical bonds such as C−C/N/O bonds and in situ formation of multiple new bonds. Indeed, such strategy could simultaneously increase the diversity of the products in a step-/atom-economic fashion. However, only a few examples have been reported to date for this issue.[11] Furthermore, a

routine two-step process terminated by DG migration was mostly found in these reported C−H functionalization/DG migration reactions.[12] Therefore, it is still highly desirable to develop new types of mild redox-neutral C−H functionalization/DG migration sequences involving multi-step (*e. g.*, three-step or four-step) cascade reactions to provide higher bond-forming efficiency and more promising synthetic applications for the construction of privileged complex skeletons.

**Scheme 1**. TM-catalyzed C−H functionalization with the assistance of DGs

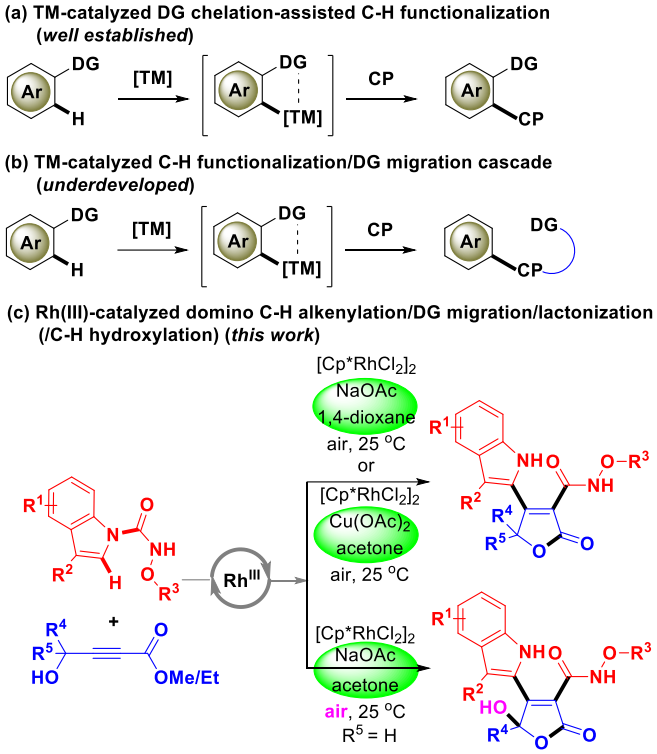


In continuation of our interest in TM (Rh, Ir, Ru)-catalyzed C−H functionalization[5e,10a-b,13] and chemodivergent synthesis triggered by C−H activation,[6a,14] herein, we disclose an unprecedented C−H coupling of *N*-carbamoyl indoles[15,16] and 4-hydroxy-2-alkynoates[17] for the synthesis of highly functionalized furan-2(5*H*)-ones via the cleavage of the more challenging C–N bond and the formation of multiple bonds at room temperature (Scheme 1c). Alternatively, an additional C5–H hydroxylation is also realized by slightly tuning the reaction solvent or additive, affording

the fully substituted furan-2(5*H*)-ones with the installation of an alcohol-based $C_5$ quaternary carbon center in a controllable manner. Through a series of detailed experimental investigations together with DFT calculations, a Rh(III)-mediated tandem C–H activation/alkyne insertion/DG migration/lactonization sequence was deduced rationally. Besides, the dual role of carbamoyl group, the principle of the selectivity as well as the origin of the hydroxyl group at C5 position were also clarified. Preliminary biological evaluation probed the potential of the obtained frameworks as novel and direct PPARγ ligands, which further strengthens the synthetic utility of the developed methodology. Compared with the synthesis of furan-2(5*H*)-ones via traditional multi-step reactions involving routine transformations of functional groups,[18] our method provides a more facile and robust access to the biologically important furan-2(5*H*)-one scaffold (Figure 1)[19] with high functionality through the domino reactions triggered by C−H activation. Besides, the present mechanistic insights also established a fundamental basis for the development of future C−H functionalization reactions employing the C–H activation/DG migration strategy for the step-/atom-economic construction of other privileged structural motifs.

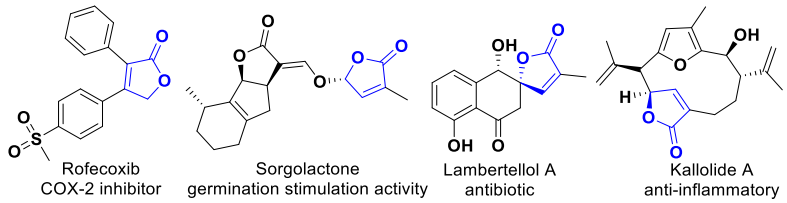


**Figure 1.** Representative bioactive compounds bearing functionalized furan-2(5*H*)-one core

## RESULTS AND DISCUSSION

**Method Development.** Optimization of the reaction conditions was performed by selecting *N*-methoxy-1*H*-indole-1-carboxamide **1aa** and methyl 4-hydroxynon-2-ynoate **2aa** as the model substrates (Table 1). Initially, **1aa** and **2aa** were treated by various TM catalysts with NaOAc as the additive in 1,4-dioxane at room temperature for 5 h under an air atmosphere (entries 1-6).

Pleasingly, the domino C−H functionalization/lactonization triggered by C−H activation between **1aa** and **2aa** occurred smoothly under the catalysis of $[Cp^*RhCl_2]_2$ with high regio- and stereoselectivity, providing *cis*-adduct **3aa** with the indole moiety exclusively located at distal *sp* hybridized carbon as the major product in a high yield (88%), along with a slight amount of the further oxidation product **4aa** (entry 6). A variety of solvents were next screened, and interestingly, a tunable reaction outcome was observed depending on the different solvents used. With low polar solvents like toluene, $CH_2Cl_2$, DCE and THF, product **3aa** was observed as the major product, while oxidation product **4aa** was selectively obtained in high polar solvents such as acetone, EtOH and DMF (entries 7-13). Gratifyingly, product **4aa** was obtained exclusively in a good yield (77%) in acetone (entry 11). Thus, with NaOAc being the additive, the Rh(III)-catalyzed solvent-controlled tandem C–H functionalization reactions were achieved, leading to the accurate synthesis of **3aa** and **4aa** in 88% and 77% yields, respectively. Further investigation on the additive effect in 1,4-dioxane[20] (entries 14-18) revealed that almost all the tested additives, among which $Cu(OAc)_2$, $Na_2CO_3$ and NaOH were also found to be effective, resulted in the formation of product **3aa** as the major product. As a comparison, a tunable additive effect was observed in acetone.[21] For example, KOAc and $Na_2CO_3$ favored product **4aa** while $Cu(OAc)_2$ and $Zn(OAc)_2$ delivered product **3aa** with a controllable manner (entries 19-23). Notably, with $Cu(OAc)_2$ being the additive, product **3aa** was obtained in a high yield (88%) with excellent chemoselectivity (entry 20). In this way, the precise synthesis of **3aa** and **4aa** was also realized in acetone in an additive-controlled manner. Taken together, the efficient Rh(III)-catalyzed solvent- or additive-controlled chemodivergent synthesis of furan-2(5*H*)-one **3aa** and 5-hydroxyfuran-2(5*H*)-one **4aa** was successfully developed via domino C–H couplings with excellent chemo-, regio- and stereoselectivity.

**Table 1.** Optimization of the reaction conditions[a]

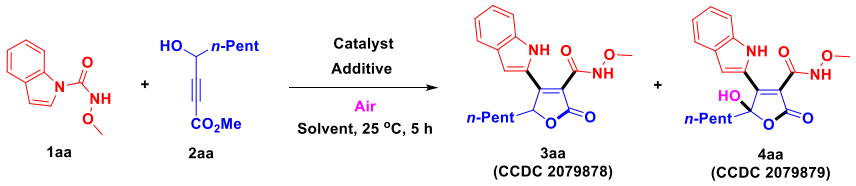


| Entry | Catalyst | Additive | Solvent | Yield of **3aa** (%)[b] | Yield of **4aa** (%)[b] |
|---|---|---|---|---|---|
| 1 | $MnBr(CO)_5$ | NaOAc | 1,4-dioxane | 0 | 0 |
| 2 | $Pd(OAc)_2$ | NaOAc | 1,4-dioxane | 0 | 0 |
| 3 | $[Cp^*IrCl_2]_2$ | NaOAc | 1,4-dioxane | <5 | 0 |
| 4 | $[RuCl_2(p\text{-cym})]_2$ | NaOAc | 1,4-dioxane | <5 | 0 |
| 5 | $CoCp_2^*PF_6$ | NaOAc | 1,4-dioxane | 0 | 0 |
| **6** | **$[Cp^*RhCl_2]_2$** | **NaOAc** | **1,4-dioxane** | **88** (77[c]) | **<5** (trace[c]) |
| 7 | $[Cp^*RhCl_2]_2$ | NaOAc | Toluene | 60 | trace |
| 8 | $[Cp^*RhCl_2]_2$ | NaOAc | $CH_2Cl_2$ | 71 | <5 |
| 9 | $[Cp^*RhCl_2]_2$ | NaOAc | DCE | 70 | <5 |
| 10 | $[Cp^*RhCl_2]_2$ | NaOAc | THF | 54 | 35 |
| **11** | **$[Cp^*RhCl_2]_2$** | **NaOAc** | **Acetone** | **trace** | **77** |
| 12 | $[Cp^*RhCl_2]_2$ | NaOAc | EtOH | 0 | 58 |
| 13 | $[Cp^*RhCl_2]_2$ | NaOAc | DMF | 0 | 22 |
| 14 | $[Cp^*RhCl_2]_2$ | KOAc | 1,4-dioxane | 36 | 42 |
| 15 | $[Cp^*RhCl_2]_2$ | $Cu(OAc)_2$ | 1,4-dioxane | 85 | 0 |
| 16 | $[Cp^*RhCl_2]_2$ | $Na_2CO_3$ | 1,4-dioxane | 79 | 0 |
| 17 | $[Cp^*RhCl_2]_2$ | NaOH | 1,4-dioxane | 67 | <5 |
| 18 | $[Cp^*RhCl_2]_2$ | NaOPiv | 1,4-dioxane | 51 | 24 |
| 19 | $[Cp^*RhCl_2]_2$ | KOAc | Acetone | 0 | 62 |
| **20** | **$[Cp^*RhCl_2]_2$** | **$Cu(OAc)_2$** | **Acetone** | **88** | **<5** |

| | | | | | |
|---|---|---|---|---|---|
| 21 | $[Cp^*RhCl_2]_2$ | $Zn(OAc)_2$ | Acetone | 67 | <5 |
| 22 | $[Cp^*RhCl_2]_2$ | $Na_2CO_3$ | Acetone | trace | 73 |
| 23 | $[Cp^*RhCl_2]_2$ | KF | Acetone | 50 | 20 |

[a]Reaction conditions: **1aa** (0.25 mmol), **2aa** (0.325 mmol), catalyst (5 mol%), additive (0.25 mmol), air (1 atm), solvent (4.0 mL), 25 °C, 5 h. [b]Isolated yield. [c]$[Cp^*RhCl_2]_2$ (2.5 mol%) was used.

**Scope for the Synthesis of Furan-2(5*H*)-ones.** With the optimized conditions in hand, we were next intrigued to explore the generality and substrate compatibility of the developed protocol. Initially, the scope of the Rh(III)-catalyzed domino reactions was investigated under the $[Cp^*RhCl_2]_2$/NaOAc/1,4-dioxane catalytic system (reaction conditions A). As shown in Scheme 2, a variety of indoles carrying diverse substituents at $R^1$-$R^3$ were tested to react with **2aa** to provide highly functionalized furan-2(5*H*)-ones with excellent regio- and stereoselectivity in good to excellent yields. For example, C4-C7 halogenated indoles reacted well to give products **3ab**-**3al** in 68-90% yields. Electron-rich indoles bearing Me, MeO or EtO at C4-C7 positions could also undergo this reaction successfully to deliver products **3am**-**3at** in 66-99% yields. To our delight, indoles bearing a heterocycle such as furan or thiophene ring at C5 position were also converted into the corresponding products **3au** and **3av** in 85% and 89% yields, respectively. Similarly, the reactions of electron-deficient indoles possessing CN, $CO_2Me$ or $CF_3$ at C5 position took place uneventfully to afford products **3aw**-**3ay** in 57-95% yields. By contrast, $NO_2$-substituted indole substrate proved unreactive but with the recovery of the starting materials. Further examination implied that indoles carrying substituents (Me, $CH_2CO_2Et$) at C3 position could also undergo this transformation to deliver the desired products **3ba** and **3bb**, albeit with lower yields. This is probably due to the steric hindrance near the reaction site caused by the C3 substituents. Indoles

owning diverse alkyl groups (Et, *i*-Pr, *t*-Bu, Bn) at $R^3$ were also proved to be suitable substrates, which participated in this reaction smoothly to produce products **3bc**-**3bf** in 36-98% yields. Gratifyingly, pyrrole substrates were also tolerated to provide the desired products **3bg** and **3bh** in good yields (42-64%). While 4-azaindole and 7-azaindole failed to undergo the desired domino reaction, which was probably mainly due to the potent coordination of pyridine-type nitrogen with $[Cp^*RhCl_2]_2$ to result in the deactivation of catalyst. Interestingly, when *N*-carbamoyl carbazole was employed, a domino C1–H alkenylation/lactonization/DG cleavage process occurred alternatively instead of the DG migration/lactonization cascade, delivering product **3bk** in 50% yield.

Subsequently, the scope of 4-hydroxy-2-alkynoates was examined to further probe the reaction compatibility. Overall, various 4-hydroxy-2-alkynoates bearing diverse substituents at $R^4$-$R^6$ could interact with **1aa** to afford highly functionalized furan-2(5*H*)-ones with excellent regio- and stereoselectivity in good to high yields. For instance, methyl 4-hydroxybut-2-ynoate, which has no substituents at $R^4$ and $R^5$, took part in this reaction to give product **3bl** in 82% yield. Expectedly, the reactions of 4-hydroxy-2-alkynoates carrying an alkyl group at C4 position appeared to be reactive, and the desired products **3bm**-**3bo** were prepared in 62-78% yields. Likewise, the reactions of C4 aryl-substituted 4-hydroxy-2-alkynoates also worked well to provide products **3bp**-**3bu** in moderate to good yields (27-78%). Interestingly, C4 cyclobutyl-substituted 4-hydroxy-2-alkynoate also turned out to be a suitable reaction component, which reacted successfully with several indole partners to give spiroproducts **3bv**-**3bx** in 42-54% yields. This process could also be applicable to sterically hindered 4-hydroxy-2-alkynoate possessing two phenyl groups at C4 position, although the desired product **3by** was synthesized in 22% yield. Of note, the desired furan-2(5*H*)-one products **3** could also be synthesized with the catalytic system

consisting of $[Cp^*RhCl_2]_2$/$Cu(OAc)_2$/acetone (reaction conditions B), of which much higher yields were observed for some cases (*e.g*. **3ae**, **3ag**, **3ah**) in comparison with conditions A. Taken together, these results demonstrated the profound compatibility of the developed protocol for the specific construction of furan-2(5*H*)-one framework.

**Scheme 2**. Scope of Rh(III)-catalyzed domino C–H alkenylation/DG migration/lactonization[a,b]

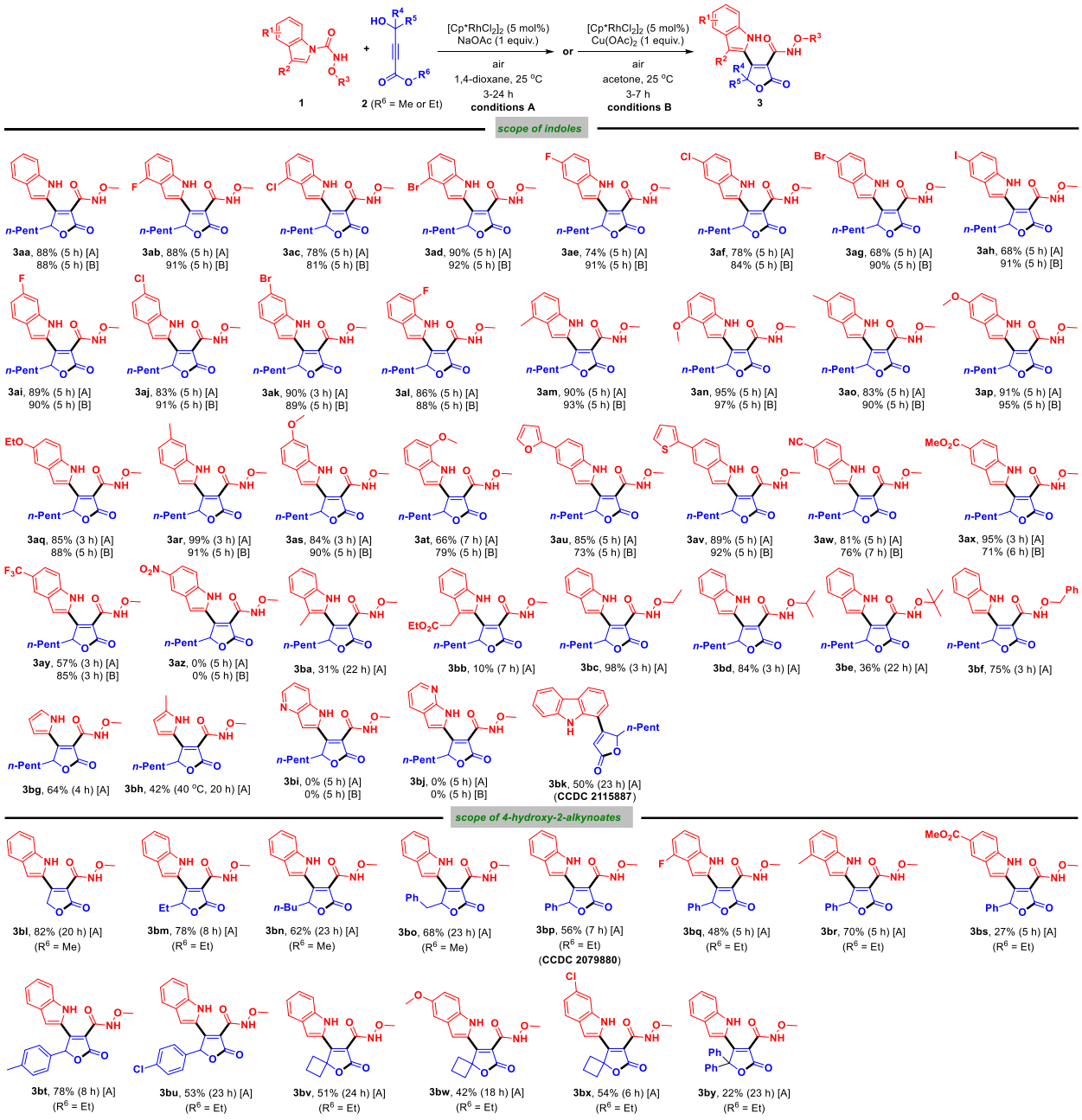


[a]Reaction conditions A: **1** (0.25 mmol), **2** (0.325 mmol), $[Cp^*RhCl_2]_2$ (5 mol%), NaOAc (0.25 mmol), air (1 atm), 1,4-dioxane (4.0 mL), 25 °C, 3-24 h. Reaction conditions B: **1** (0.25 mmol), **2** (0.325 mmol), $[Cp^*RhCl_2]_2$ (5 mol%), $Cu(OAc)_2$ (0.25 mmol), air (1 atm), acetone (4.0 mL), 25 °C, 3-7 h. [b]Isolated yield.

**Scope for the Synthesis of 5-Hydroxyfuran-2(5*H*)-one Derivatives.** Having established the efficient Rh(III)-catalyzed domino C–H couplings for the synthesis of various furan-2(5*H*)-ones, we then examined the substrate scope for the chemoselective construction of 5-hydroxyfuran-2(5*H*)-ones with the catalytic system of $[Cp^*RhCl_2]_2$/NaOAc/acetone (reaction conditions C). Generally, a variety of indoles bearing diverse substituents at $R^1$-$R^3$ and a diversity of 4-hydroxy-2-alkynoates carrying various substituents at $R^4$-$R^5$ were well tolerated (Scheme 3), producing the desired 5-hydroxyfuran-2(5*H*)-ones with excellent regio- and stereoselectivity in moderate to high yields. The scope of indoles was checked at first with **2aa** as the coupling partner. For example, the reactions of C4-C7 halogenated indoles worked well to deliver products **4ab**-**4al** in 40-75% yields. Electron-rich indoles having Me, MeO or EtO at C4-C7 positions reacted smoothly to provide products **4am**-**4au** in 25-90% yields. The reactions of indoles bearing a furan or thiophene ring at C5 position proceeded well to give products **4av** and **4aw** in 46% and 71% yields, respectively. Electron-deficient indoles having CN, $CO_2Me$ or $CF_3$ at C5 position were uneventfully converted into the corresponding products **4ax**-**4az** in 66-74% yields. Indoles owning substituents (Me, Bn) at C3 position could also undergo this transformation, although the desired products **4bb** and **4bc** were obtained in lower yields. Moreover, this reaction was also compatible with indoles possessing diverse alkyl groups (Et, *i*-Pr, *t*-Bu, Bn) at $R^3$, which reacted well to afford products **4bd**-**4bg** in 50-78% yields. However, 4-azaindole and 7-azaindole substrates were also not tolerated, but with the recovery of starting materials. Of note, the reactions of *N*-carbamoyl pyrroles or *N*-carbamoyl carbazole resulted in the formation of furan-2(5*H*)-one derivatives rather than 5-hydroxyfuran-2(5*H*)-ones under conditions C, suggesting that the nature of the substrates had an effect on further oxidation process from furan-2(5*H*)-one.

Next, the scope of 4-hydroxy-2-alkynoates was studied with **1aa** as the reaction partner. For instance, various C4 alkyl-substituted 4-hydroxy-2-alkynoates participated in this reaction successfully to provide products **4bk**-**4bm** in 36-69% yields. Likewise, diverse C4 aryl-substituted 4-hydroxy-2-alkynoates underwent this transformation smoothly to give products **4bn**-**4bs** in 51-82% yields.

**Scheme 3**. Scope of Rh(III)-catalyzed domino C–H alkenylation/DG migration/lactonization/C–H hydroxylation[a,b]

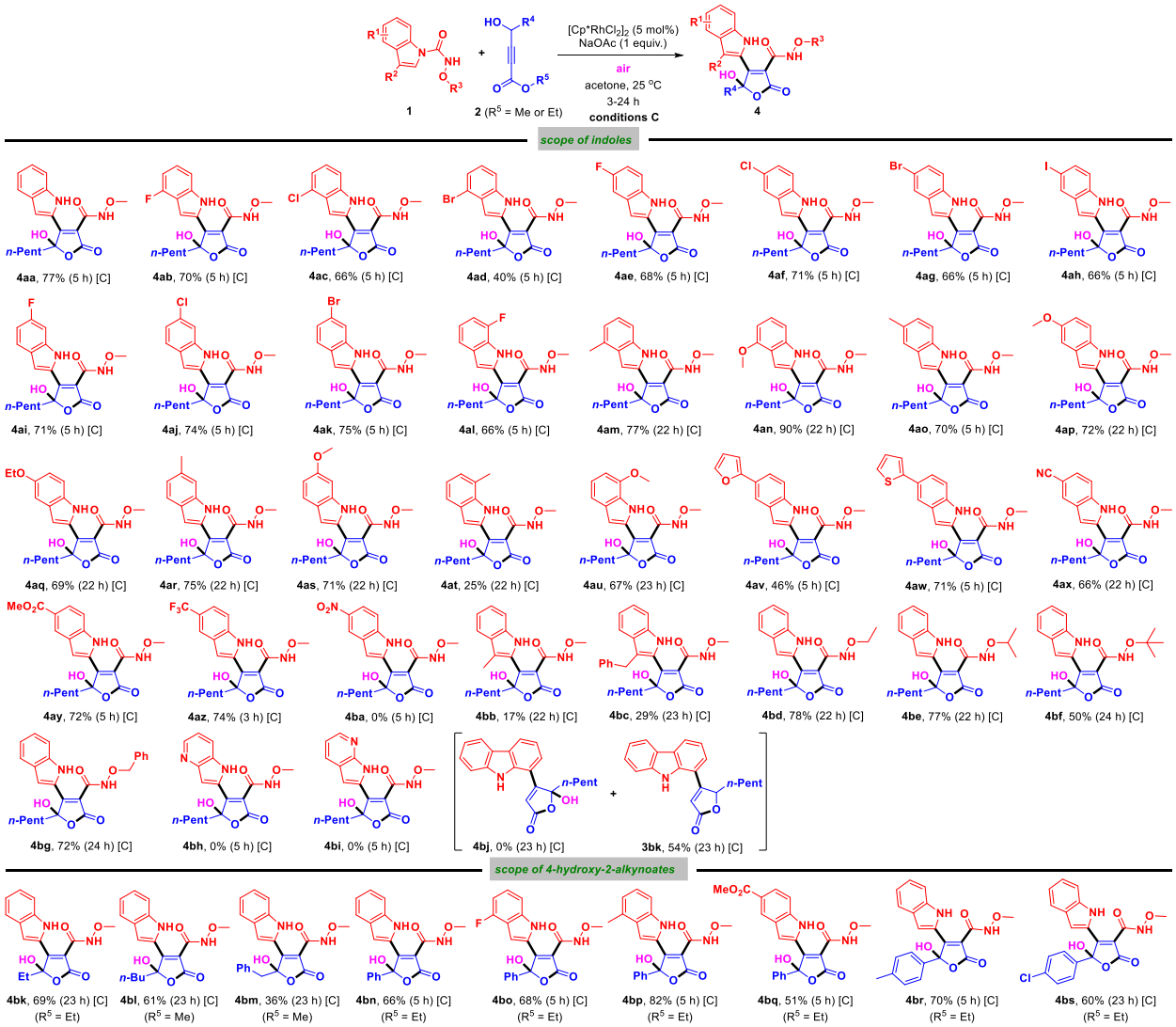

[a]Reaction conditions C: **1** (0.25 mmol), **2** (0.325 mmol), $[Cp^*RhCl_2]_2$ (5 mol%), NaOAc (0.25 mmol), air (1 atm), acetone (4.0 mL), 25 °C, 3-24 h. [b]Isolated yield.

To further demonstrate the synthetic availability of the developed methodology, the two domino reactions triggered by C−H activation were carried out at gram scales for the precise synthesis of both **3aa** and **4aa** (Scheme S1). Impressively, both reactions could be easily scale up without the loss of efficiency, suggesting the synthetic practicality and industrial prospects of this protocol. An investigation of various directing groups disclosed that both the free hydrogen and alkoxy group tethered to the carbamoyl nitrogen atom are essential to fulfill the observed reaction manifolds (Scheme S2). In view of the intriguing indole-tethered furan-2(5*H*)-one and 5-hydroxyfuran-2(5*H*)-one structures, a further exploration of their pharmaceutical applications was also carried out. In continuation of our interest in developing novel PPARγ ligands[22] including indole derivatives for PPARγ-based drug discovery, the obtained compounds were screened by LanthaScreen™ TR-FRET assay to probe their binding affinity to PPARγ. The results revealed that potent binding affinity of both the selected furan-2(5*H*)-ones and 5-hydroxyfuran-2(5*H*)-ones to PPARγ were observed (Figure S1), thus providing a basis for further evaluation of such molecules as candidate compounds for the potent treatment of PPARγ-based disorders, such as type 2 diabetes mellitus.

**Experimental Mechanistic Studies.** Given the novel and distinctive reaction modes enabled by the solvent- or additive-controlled domino C–H functionalization, we were next intrigued to disclose the reaction mechanism, in particular, to clarify the reaction sequence and probe the role of the solvent and additive in tuning the reaction outcome. Firstly, a set of control experiments were performed to confirm the source of oxygen in the oxidation product **4aa**. As shown in Scheme 4a-c, the reaction of **1aa** and **2aa** was carried out under both conditions A or C under the

atmosphere of $N_2$, as a result, the formation of **4aa** was obviously suppressed, implying that the air atmosphere was essential for providing **4aa**. Inspired by this finding, a further control experiment under conditions C using $^{18}O_2$ resulted in the formation of $^{18}O$-labled **4aa** in 81% yield (Scheme 4d), which further confirmed that the 5-hydroxyfuran-2(5*H*)-one product **4aa** was oxidized from furan-2(5*H*)-one skeleton by $O_2$. Interestingly, when the reaction of **1aa** and **2aa** was carried out under conditions A even under $O_2$ atmosphere, the oxidation product **4aa** was still obtained as a minor product with less than 5% yield (Scheme 4e). This result revealed that the solvent acetone was important for the formation of **4aa**, and this might be attributed to the much better solubility of $O_2$ in acetone than that in 1,4-dioxane.[23]

**Scheme 4**. Control experiments between **1aa** and **2aa**

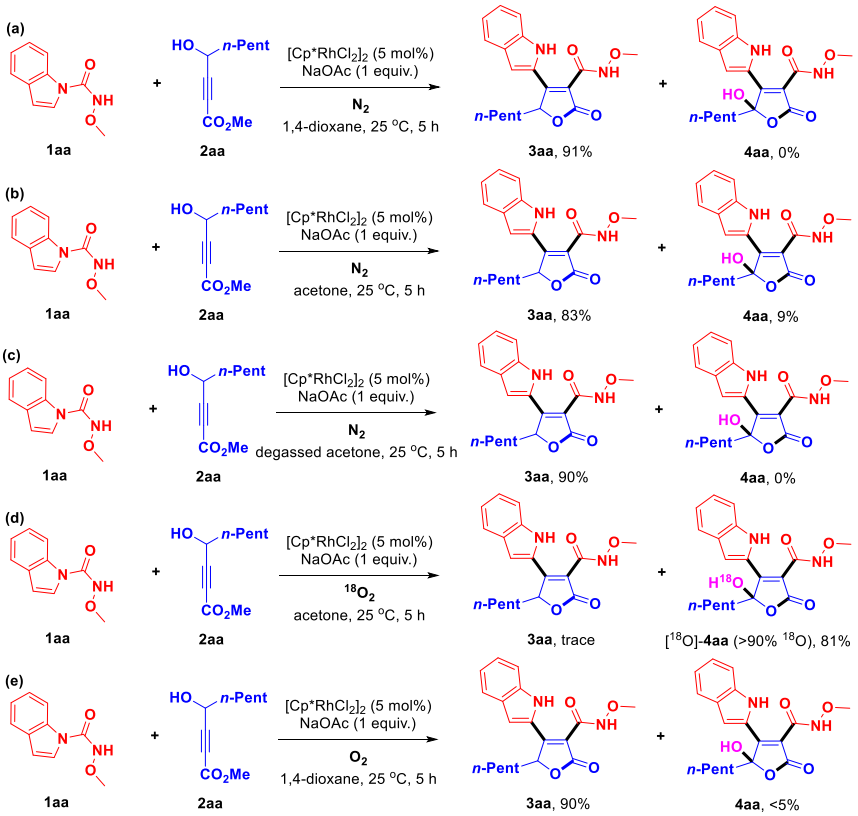

To get a better understanding of the oxidation process, additional control experiments were next conducted starting from **3aa** (Table 2). Preliminary screening revealed that **3aa** failed to convert into **4aa** in the presence of air or $[Cp^*RhCl_2]_2$ only, while the NaOAc additive was crucial in prompting this oxidation process although a long reaction time (32 h) was required to complete the transformation to afford product **4aa** in 86% yield (entries 1-3). The combination of $[Cp^*RhCl_2]_2$ and NaOAc was proved to be beneficial for the oxidation reaction and shorten the reaction time to 12 h with 87% yield of **4aa** (entry 4). Moreover, the addition of DABCO, a singlet oxygen inhibitor,[24] into the reaction mixture could not inhibit the reaction, similar result was obtained when the reaction was conducted in dark (entries 5-6). These results suggested that singlet molecular oxygen was not likely to be involved. The addition of radical inhibitors such as TEMPO and BHT had no impact on this transformation, suggesting that the radical species was not involved (entries 7-8). Subsequent screening of other additives showed that neutral salts such as NaCl, $Cu(OAc)_2$ and $Zn(OAc)_2$ were all ineffective, while basic salts *e.g.* CsOAc, KOAc, $Na_2CO_3$ and $K_2CO_3$ promoted the oxidation efficiently (entries 9-15). Thus, a base-mediated oxidation from **3aa** into **4aa** might be involved.

**Table 2**. Study on the oxidation conversion of **3aa** to **4aa**[a]

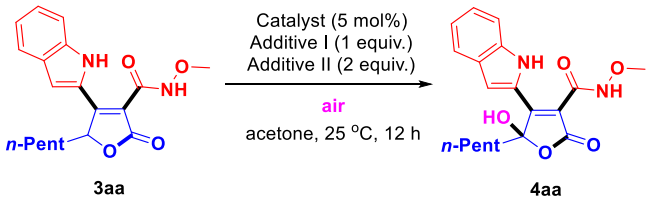


| Entry | Catalyst | Additive I | Additive II | Yield of **4aa** (%)[b] |
|---|---|---|---|---|
| 1 | - | - | - | 0 |
| 2 | $[Cp^*RhCl_2]_2$ | - | - | 0 |

| | | | | |
|---|---|---|---|---|
| 3 | - | NaOAc | - | 58(86[c]) |
| 4 | $[Cp^*RhCl_2]_2$ | NaOAc | - | 87 |
| 5 | $[Cp^*RhCl_2]_2$ | NaOAc | DABCO | 87 |
| 6 | $[Cp^*RhCl_2]_2$ | NaOAc | in dark | 85 |
| 7 | $[Cp^*RhCl_2]_2$ | NaOAc | TEMPO | 81 |
| 8 | $[Cp^*RhCl_2]_2$ | NaOAc | BHT | 83 |
| 9 | - | NaCl | - | 0 |
| 10 | - | $Cu(OAc)_2$ | - | 0 |
| 11 | - | $Zn(OAc)_2$ | - | 0 |
| 12 | - | CsOAc | - | 89 |
| 13 | - | KOAc | - | 88 |
| 14 | - | $Na_2CO_3$ | - | 84 |
| 15 | - | $K_2CO_3$ | - | 85 |

[a]Reaction conditions: **3aa** (0.125 mmol), catalyst (5 mol%), additive I (0.125 mmol), additive II (0.25 mmol), air (1 atm), acetone (4.0 mL), 25 °C, 12 h. [b]Isolated yield. [c]Data after 32 h. DABCO = 1,4-diazabicyclo[2,2,2]octane; TEMPO = 2,2,6,6-tetramethylpiperidine-1-oxyl; BHT = 2,6-di-*tert*-butyl-4-methylphenol.

To rationalize the reaction mechanism, deuterium-labeling experiments were also performed with **1aa** in $CD_3OD$ under standard conditions (Scheme 5a). The results of H/D scrambling at C2, C3 and C7 positions of the indole ring suggested the reversible nature of the C–H bond cleavage.[25] In addition, a low KIE value of 1.21 obtained by KIE study indicated that the step of C–H bond cleavage was unlikely to be rate-limiting (Scheme 5b). Competition experiments between electronically different indoles showed that electron-deficient indole was favored, suggesting that the C–H bond cleavage may occur via a concerted metalation-deprotonation (CMD) mechanism (Scheme 5c).[26] Further control experiments revealed that the desired domino reaction occurred

smoothly to afford furan-2(5*H*)-one **3aa** under Cp*Rh(OAc)$_2$/1,4-dioxane catalytic system in the absence of external additives, suggesting Cp*Rh(OAc)$_2$ could be the active catalyst for this transformation. Additionally, only a slight amount of 5-hydroxyfuran-2(5*H*)-one **4aa** was detected under Cp*Rh(OAc)$_2$/acetone catalytic system, further revealing that the base additive was critical for the oxidation process (Scheme 5d).

**Scheme 5**. Mechanistic Studies

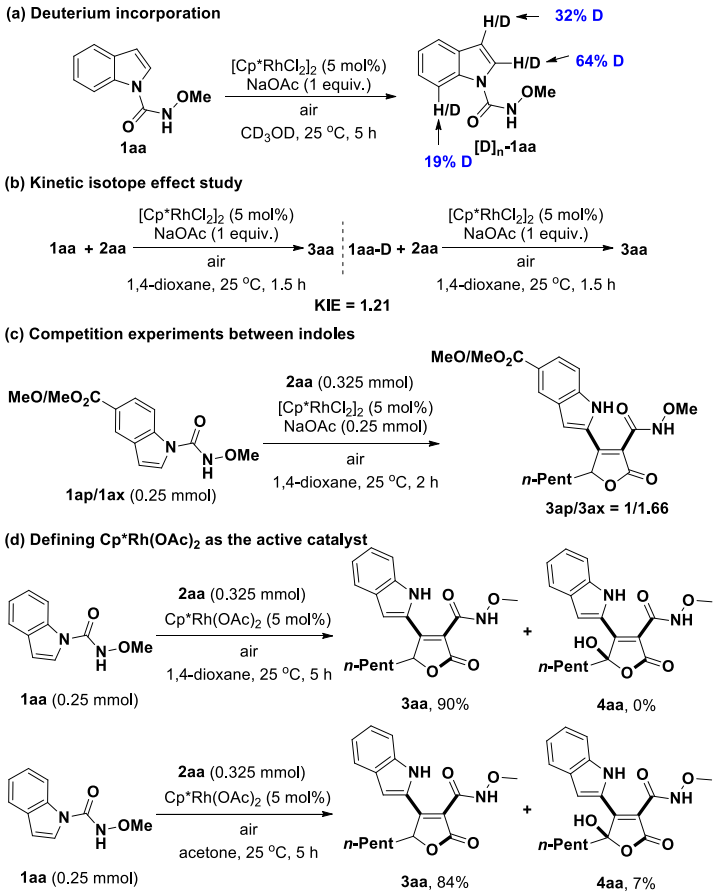


**Computational Mechanistic Studies.** To further probe the reaction path, in particular, to clarify the DG migration and lactonization processes, detailed DFT calculations were next carried out by rationally selecting the active Cp*Rh(OAc)$_2$ catalyst as the starting point (Figure 2). Briefly, all the structures were optimized at the B3LYP level in 1,4-dioxane (see the supporting information

for details). Initially, the coordination of indole substrate **1aa** with Cp*Rh(OAc)$_2$ afforded intermediate **INT-1**, followed by the sequential N−H/C−H cleavage via **TS-1** and **TS-2** with an energy barrier of 8.3 kcal/mol (from **INT-1** to **TS-2**). The five-membered rhodacycle **INT-4** was formed with a free energy of -4.9 kcal/mol. Obviously, the low energy barriers for C−H metallation and the corresponding reverse reaction suggested an reversible C−H bond activation process, which was in line with the deuterium incorporation experiment and the kinetic isotope study. The subsequent regioselective alkyne coordination followed by the insertion into C–Rh bond via **TS-3** ($\Delta G^{\neq}$ = 2.6 kcal/mol) occurred to afford intermediate **INT-7**, while a relatively high energy barrier was involved via **TS-3'** ($\Delta G^{\neq}$ = 9.5 kcal/mol) for the contrary insertion mode (17.5 *vs* 10.4 kcal/mol), which accounted for the observed regioselectivity.

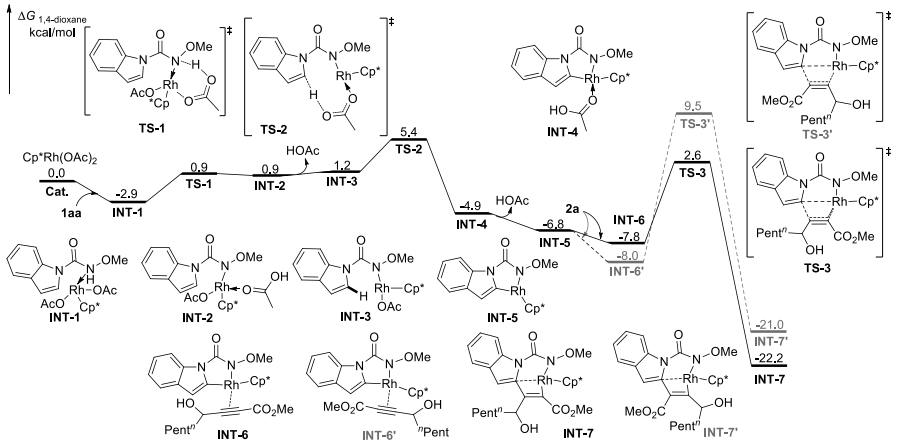


**Figure 2.** Computed Gibbs free energy changes of the reaction pathway for C−H activation and alkyne insertion.

From **INT-7**, the protonolysis of N–Rh bond followed by a conformational change led to the formation of **INT-9** (Figure 3), which underwent the intramolecular nucleophilic addition of C–Rh bond into the carbonyl moiety with an energy barrier of 26.3 kcal/mol (from **INT-7** to **TS-4**), affording intermediate **INT-10** with a free energy of -12.4 kcal/mol. The following ring-opening

process via **TS-5** ($\Delta G^{\neq}$ = 1.4 kcal/mol) delivered the DG migration intermediate **INT-11** with a free energy of -14.4 kcal/mol. As a comparison, a relatively high energy barrier of 28.7 kcal/mol (from **INT-7** to **TS-4a**) was involved for the direct C–N reductive elimination process, which was in consistent with the observed chemoselectivity that only DG migration rather than pyrimidoindolone product was detected. The lactonization from **INT-11** was next clarified, and an intramolecular transesterification process was first ruled out due to the high energy barrier of 35.9 kcal/mol (from **INT-11** to **TS-6b**). Alternatively, a more stable intermediate **INT-12** ($\Delta G^{\neq}$ = -18.9 kcal/mol) was facilely generated due to the potent affinity between rhodium metal center and the hydroxyl group, which converted into **INT-13** via a proton transfer process with an energy barrier of 15.6 kcal/mol (from **INT-12** to **TS-6**). Subsequent lactonization occurred smoothly via **TS-7** and **TS-8** bearing the energy barriers of 5.2 kcal/mol (from **INT-14** to **TS-7**) and 1.4 kcal/mol (from **INT-15** to **TS-8**), respectively, yielding the final product with a free energy of -41.8 kcal/mol. A metal-free lactonization process was also excluded due to the high energy barrier of 32.1 kcal/mol (from **INT-12c** to **TS-6c**), demonstrating that the rhodium-mediated lactonization was more reasonable.

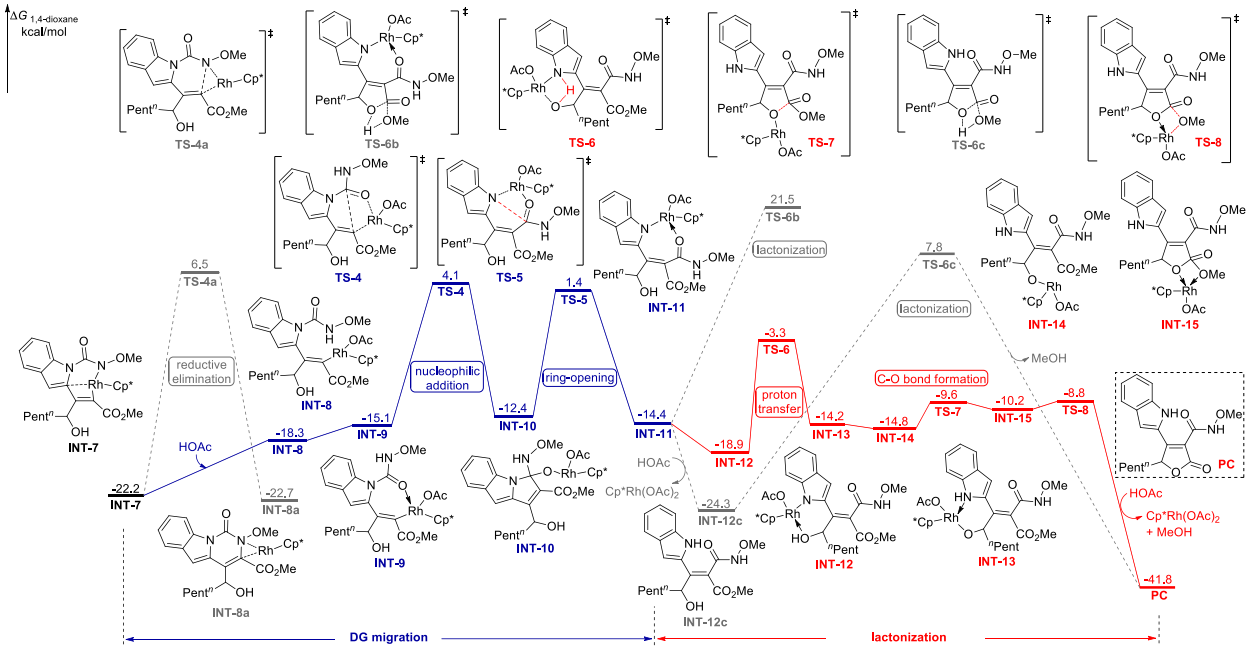


**Figure 3.** Computed Gibbs free energy changes of the reaction pathway for DG migration and lactonization.

Subsequently, the reaction sequence was rationalized by comparing the computed Gibbs free energy profiles of different reaction pathways (Figure S2). Instead of the DG migration/lactonization sequence presented in Figure 3, an alternative lactonization from **INT-7** proceeded via **TS-4d** ($\Delta G^{\neq}$ = 7.9 kcal/mol) to afford **INT-9d**, which further converted into a more stable intermediate **INT-10d** along with the release of MeOH. Further protonolysis of N–Rh bond followed by intramolecular nucleophilic addition via **TS-5d** ($\Delta G^{\neq}$ = 4.3 kcal/mol) led to the formation of **INT-13d**. The high energy barriers of 32.5 kcal/mol (from **INT-8d** to **TS-4d**) and 40.4 kcal/mol (from **INT-10d** to **TS-5d**) implied that this lactonization/DG migration reaction sequence might be unreasonable. Moreover, other lactonization modes from **INT-8** or **INT-10** were also ruled out due to the high energy barrier (31.3 kcal/mol from **INT-8** to **TS-4e**, 42.0 kcal/mol from **INT-10** to **TS-5g**). Taken together, these results provided adequate evidence to support a C–H activation/alkyne insertion/DG migration/lactonization reaction sequence for the

developed transformation. Additionally, in view of the nature of the substrate, we carried out further DFT calculations for the kinetic limiting steps with different indoles. The results showed similar energy profiles despite of the electronic properties of the substituents on the indole ring or the steric hindrance of the alkoxyl group tethered to the nitrogen atom, which was in accordance with the observed good substrate compatibility and broad functional group tolerance (Figure S3-S5).

**Scheme 6.** Proposed reaction mechanism

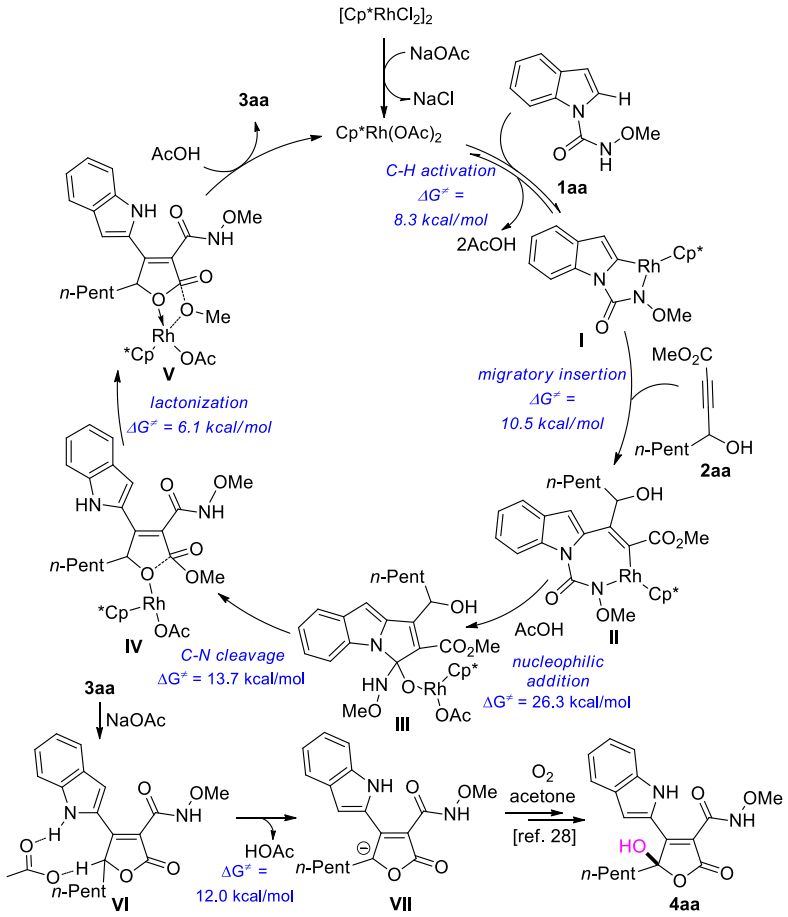


**Mechanistic Proposal.** A putative reaction mechanism was proposed in Scheme 6 based on the above mechanistic studies and literature precedents.[11,27] An active catalyst $Cp^*Rh(OAc)_2$ is initially generated via ligand exchange in the presence NaOAc. The following chelation-assisted

reversible C−H activation occurs to give intermediate **I**. Subsequently, intermediate **II** is produced by the regiospecific migratory insertion of alkyne **2aa** into the Rh–C bond of intermediate **I**. The polarization of the C≡C bond by the ester group accounts for the observed regioselectivity, which has been confirmed by the DFT calculations (**TS-3** *vs* **TS-3'**). Then, the intramolecular nucleophilic addition occurs from intermediate **II** to afford intermediate **III**, which undergoes C–N bond cleavage and intramolecular hydrogen transfer to afford intermediate **IV**. Finally, the lactonization proceeds from intermediate **IV** to provide product **3aa** along with the regeneration of the active rhodium complex via intermediate **V**. With the assistance of NaOAc, the cleavage of the allylic C-H bond in **3aa** occurred smoothly, furnishing intermediate **VII** with an energy barrier of 12.0 kcal/mol (see Figure S6 in the supporting information for details), which could be further oxidized in the presence of $O_2$ in acetone[28] to give the 5-hydroxyfuran-2(5*H*)-one product **4aa**.

## CONCLUSIONS

In conclusion, by giving the carbamoyl DG a dual role of auxiliary group and migrating acylating reagent, we have developed a mild redox-neutral Rh(III)-catalyzed domino C–H alkenylation/DG migration/lactonization between *N*-carbamoyl indoles and 4-hydroxy-2-alkynoates for the direct assembly of highly functionalized furan-2(5*H*)-ones at room temperature. More importantly, the obtained furan-2(5*H*)-one skeleton could further undergo C5–H hydroxylation under air in situ by simply changing the solvent or additive, providing the fully substituted furan-2(5*H*)-ones bearing an alcohol-based $C_5$ quaternary carbon center. The protocol features efficient multi-step cascade triggered by C−H activation, excellent chemo-, regio- and stereoselectivity, high bond-forming efficiency, superior step- and atom-economy, good functional group compatibility and mild redox-neutral conditions. The dual role of carbamoyl group, the origin of the selectivity and the reaction pathway were rationally clarified by a combined experimental and DFT study. Furthermore, the

biological application in evaluating these obtained furan-2(5*H*)-ones as a potent class of PPARγ ligands was also successfully demonstrated, suggesting that further development of such types of compounds might be of interest for the potent treatment of PPARγ-based disorders. Further development of novel domino C−H functionalization reactions by using such strategy and their applications for drug discovery are in progress.

## ASSOCIATED CONTENT

## AUTHOR INFORMATION


### Corresponding Author

*E-mail: zhaofei@cdu.edu.cn

*E-mail: wuxiaowei@simm.ac.cn

*E-mail: yiwei@gzhmu.edu.cn


### Author Contributions

[#]These authors contributed equally.

### Notes

The authors declare no competing financial interest.

### Supporting Information.

The Supporting Information is available free of charge at the ACS Publications website.

Experimental procedures, characterization of products, computational details, and copies of $^{1}H$ and $^{13}C$ spectra (PDF)

Crystallographic data of compound **3aa** (CIF)

Crystallographic data of compound **4aa** (CIF)

Crystallographic data of compound **3bk** (CIF)

Crystallographic data of compound **3bp** (CIF)

ACKNOWLEDGMENT

We gratefully acknowledge the financial support from National Natural Science Foundation of China (Grant 21602022, 21877020), 1000 Talents Program of Sichuan Province, Chengdu Talents Program, Chenghua District Talents Program, Science and Technology Program of Sichuan Province (Grant 2018JY0345), Guangdong Natural Science Funds for Distinguished Young Scholar (2017 A030306031) and Shanghai Pujiang Program (21PJ1415800).

REFERENCES

(1) (a) Collet, F.; Dodd, R. H.; Dauban, P. Catalytic C–H Amination: Recent Progress and Future Directions. *Chem. Commun.* **2009**, 5061−5074. (b) Cho, S. H.; Kim, J. Y.; Kwak, J.; Chang, S. Recent Advances in the Transition Metal-Catalyzed Twofold Oxidative C–H Bond Activation Strategy for C–C and C–N Bond Formation. *Chem. Soc. Rev.* **2011**, *40*, 5068−5083. (c) Ramirez, T. A.; Zhao, B.; Shi, Y. Recent Advances in Transition Metal-Catalyzed $sp^3$ C–H Amination Adjacent to Double Bonds and Carbonyl Groups. *Chem. Soc. Rev.* **2012**, *41*, 931−942. (d) Colby, D. A.; Tsai, A. S.; Bergman, R. G.; Ellman, J. A. Rhodium Catalyzed Chelation-Assisted C–H Bond Functionalization Reactions. *Acc. Chem. Res*. **2012**, *45*, 814−825. (e) Wencel-Delord, J.; Glorius, F. C–H Bond Activation Enables the Rapid Construction and Late-Stage Diversification of Functional Molecules. *Nat. Chem*. **2013**, *5*, 369−375. (f) Ros, A.; Fernández, R.; Lassaletta, J. M. Functional Group Directed C–H Borylation. *Chem. Soc. Rev.* **2014**, *43*, 3229−3243. (g) Han,

Y.-F.; Jin, G.-X. Cyclometalated [Cp*M(C^X)] (M = Ir, Rh; X = N, C, O, P) Complexes. *Chem. Soc. Rev*. **2014**, *43*, 2799−2823. (h) Chen, Z.; Wang, B.; Zhang, J.; Yu, W.; Liu, Z.; Zhang, Y. Transition Metal-Catalyzed C–H Bond Functionalizations by the Use of Diverse Directing Groups. *Org. Chem. Front.* **2015**, *2*, 1107−1295. (i) Davies, D. L.; Macgregor, S. A.; McMullin, C. L. Computational Studies of Carboxylate-Assisted C–H Activation and Functionalization at Group 8–10 Transition Metal Centers. *Chem. Rev*. **2017**, *117*, 8649−8709. (j) Xue, X. S.; Ji, P.; Zhou, B.; Cheng, J. P. The Essential Role of Bond Energetics in C–H Activation/Functionalization. *Chem. Rev.* **2017**, *117*, 8622−8648. (k) He, J.; Wasa, M.; Chan, K. S. L.; Shao, Q.; Yu, J.-Q. Palladium-Catalyzed Transformations of Alkyl C–H Bonds. *Chem. Rev*. **2017**, *117*, 8754−8786. (l) Park, Y.; Kim, Y.; Chang, S. Transition Metal-Catalyzed C–H Amination: Scope, Mechanism, and Applications. *Chem. Rev*. **2017**, *117*, 9247−9301. (m) Shan, C.; Zhu, L.; Qu, L. B.; Bai, R.; Lan, Y. Mechanistic View of Ru-Catalyzed C–H Bond Activation and Functionalization: Computational Advances. *Chem. Soc. Rev.* **2018**, *47*, 7552−7576. (n) Gensch, T.; James, M. J.; Dalton, T.; Glorius, F. Increasing Catalyst Efficiency in C−H Activation Catalysis. *Angew. Chem. Int. Ed*. **2018**, *57*, 2296−2306. (o) Chen, Z.; Rong, M. Y.; Nie, J.; Zhu, X. F.; Shi, B. F.; Ma, J. A. Catalytic Alkylation of Unactivated C($sp^3$)–H Bonds for C($sp^3$)–C($sp^3$) Bond Formation. *Chem. Soc. Rev.* **2019**, *48*, 4921−4942. (p) Song, L.-R.; Fan, Z.; Zhang, A. Recent Advances in Transition Metal-Catalyzed C($sp^2$)–H Nitration. *Org. Biomol. Chem.* **2019**, *17*, 1351−1361. (q) Gandeepan, P.; Müller, T.; Zell, D.; Cera, G.; Warratz, S.; Ackermann, L. 3d Transition Metals for C–H Activation. *Chem. Rev.* **2019**, *119*, 2192–2452. (r) Zhao, Q.; Meng, G.; Nolan, S. P.; Szostak, M. *N*-Heterocyclic Carbene Complexes in C–H Activation Reactions. *Chem. Rev.* **2020**, *120*, 1981–2048. (s) Wu, M.-J.; Chu, J.-H. Directing Group Assists in Transition Metal-Catalyzed Site-Selective C–H Bond Activation/Transformations. *J. Chin. Chem. Soc*. **2020**, *67*, 399−421.

(2) (a) Colby, D. A.; Bergman, R. G.; Ellman, J. A. Rhodium-Catalyzed C–C Bond Formation via Heteroatom-Directed C–H Bond Activation. *Chem. Rev*. **2010**, *110*, 624−655. (b) Yoshikai, N. Cobalt-Catalyzed, Chelation-Assisted C–H Bond Functionalization. *Synlett* **2011**, 1047–1051. (c) Song, G.; Wang, F.; Li, X. C-C, C-O and C-N Bond Formation via Rhodium(III)-Catalyzed Oxidative C–H Activation. *Chem. Soc. Rev*. **2012**, *41*, 3651−3678. (d) Ackermann, L. Carboxylate-Assisted Ruthenium-Catalyzed Alkyne Annulations by C–H/Het–H Bond Functionalizations. *Acc. Chem. Res*. **2014**, *47*, 281−295. (e) Zhao, B.; Shi, Z.; Yuan, Y. Transition-Metal-Catalyzed Chelation-Assisted C–H Functionalization of Aromatic Substrates. *Chem. Rec*. **2016**, *16,* 886–896. (f) Subhedar, D. D.; Mishra, A. A.; Bhanage, B. M. *N*-Methoxybenzamide: A Versatile Directing Group for Palladium-, Rhodium- and Ruthenium-Catalyzed C−H Bond Activations. *Adv. Synth. Catal*. **2019**, *361*, 4149−4195. (g) Kuang, G.; Liu, G.; Zhang, X.; Lu, N.; Peng, Y.; Xiao, Q.; Zhou, Y. Directing-Group-Assisted Transition-Metal-Catalyzed Direct C–H Oxidative Annulation of Arenes with Alkynes for Facile Construction of Various Oxygen Heterocycles. *Synthesis* **2020**, *52*, 993−1006. (h) Zhang, J.; Lu, X.; Shen, C.; Xu, L.; Ding, L.; Zhong, G. Recent Advances in Chelation-Assisted Site- and Stereoselective Alkenyl C–H Functionalization. *Chem. Soc. Rev*. **2021**, *50*, 3263–3314.

(3) (a) Arockiam, P. B.; Bruneau, C.; Dixneuf, P. H. Ruthenium(II)-Catalyzed C–H Bond Activation and Functionalization. *Chem. Rev.* **2012**, *112*, 5879–5918. (b) Corbet, M.; Campo, F. D. 8-Aminoquinoline: A Powerful Directing Group in Metal-Catalyzed Direct Functionalization of C–H Bonds. *Angew. Chem. Int. Ed*. **2013**, *52*, 9896–9898. (c) Rouquet, G.; Chatani, N. Catalytic Functionalization of $C(sp^2)$-H and $C(sp^3)$-H Bonds by Using Bidentate Directing Groups. *Angew. Chem. Int. Ed*. **2013**, *52*, 11726−11743. (d) Liu, J.; Chen, G.; Tan, Z. Copper-Catalyzed or -Mediated C–H Bond Functionalizations Assisted by Bidentate Directing Groups. *Adv. Synth.*

*Catal*. **2016**, *358*, 1174−1194. (e) Zhou, Y.; Yuan, J.; Yang, Q.; Xiao, Q.; Peng, Y. Directing-Group-Assisted Transition-Metal-Catalyzed Direct Intermolecular C–H Amidation and Amination of Arenes. ChemCatChem **2016**, *8*, 2178–2192. (f) Shang, M.; Sun, S.-Z.; Wang, H.-L.; Wang, M.-M.; Dai, H.-X. Recent Progress on Copper-Mediated Directing-Group-Assisted C($sp^2$)–H Activation. *Synthesis* **2016**, *48*, 4381–4399. (g) Yang, X.; Shan, G.; Wang, L.; Rao, Y. Recent Advances in Transition Metal (Pd, Ni)-Catalyzed C($sp^3$)–H Bond Activation with Bidentate Directing Groups. *Tetrahedron Lett*. **2016**, *57*, 819−836. (h) Ma, W.; Gandeepan, P.; Li, J.; Ackermann, L. Recent Advances in Positional-Selective Alkenylations: Removable Guidance for Twofold C–H Activation. *Org. Chem. Front*. **2017**, *4*, 1435−1467. (i) Kommagalla, Y.; Chatani, N. Cobalt(II)-Catalyzed C–H Functionalization Using an *N*,*N*'-Bidentatedirecting Group. *Coord. Chem. Rev*. **2017**, *350*, 117–135. (j) Caspers, L. D.; Nachtsheim, B. J. Directing-Group-Mediated C−H-Alkynylations. *Chem. Asian J*. **2018**, *13*, 1231–1247. (k) Rej, S.; Ano, Y.; Chatani, N. Bidentate Directing Groups: An Efficient Tool in C–H Bond Functionalization Chemistry for the Expedient Construction of C–C Bonds. *Chem. Rev.* **2020**, *120*, 1788–1887. (l) Kapoor, M.; Singh, A.; Sharma, K.; Hsu, M. H. Site-Selective C($sp^3$)−H and C($sp^2$)−H Functionalization of Amines Using a Directing-Group-Guided Strategy. *Adv. Synth. Catal*. **2020**, *362*, 4513–4542. (m) Ghosh, K.; Rit, R. K.; Shankar, M.; Mukherjee, K.; Sahoo, A. K. Directing Group Assisted Unsymmetrical Multiple Functionalization of Arene C−H Bonds. *Chem. Rec*. **2020**, *20*, 1017–1042. (n) Fitzgerald, L. S.; O'Duill, M. L. A Guide to Directing Group Removal: 8-Aminoquinoline. *Chem. Eur. J*. **2021**, *27*, 8411–8436.

(4) For selected reviews, see: (a) Patureau, F. W.; Glorius, F. Oxidizing Directing Groups Enable Efficient and Innovative C−H Activation Reactions. *Angew. Chem. Int. Ed*. **2011**, *50*, 1977−1979. (b) Huang, H.; Ji, X.; Wu, W.; Jiang, H. Transition Metal-Catalyzed C–H Functionalization of *N*-

Oxyenamine Internal Oxidants. *Chem. Soc. Rev*. **2015**, *44*, 1155−1171. (c) Mo, J.; Wang, L.; Liu, Y.; Cui, X. Transition-Metal-Catalyzed Direct C–H Functionalization under External-Oxidant-Free Conditions. *Synthesis* **2015**, *47,* 439–459.

(5) (a) Liu, G.; Shen, Y.; Zhou, Z.; Lu, X. Rhodium(III)-Catalyzed Redox-Neutral Coupling of *N*-Phenoxyacetamides and Alkynes with Tunable Selectivity. *Angew. Chem. Int. Ed.* **2013**, *52*, 6033–6037. (b) Zhang, X.; Qi, Z.; Li, X. Rhodium(III)-Catalyzed C–C and C–O Coupling of Quinoline *N*-Oxides with Alkynes: Combination of C–H Activation with O-Atom Transfer. *Angew. Chem. Int. Ed.* **2014***, 53*, 10794–10798. (c) Chen, Y.; Wang, D.; Duan, P.; Ben, R.; Dai, L.; Shao, X.; Hong, M.; Zhao, J.; Huang, Y. A Multitasking Functional Group Leads to Structural Diversity Using Designer C–H Activation Reaction Cascades. *Nat. Commun*. **2014**, *5*, 4610. (d) Datee, R. B.; Chang, S. Selective Cyclization of Arylnitrones to Indolines under External Oxidant-Free Conditions: Dual Role of Rh(III) Catalyst in the C–H Activation and Oxygen Atom Transfer. *J. Am. Chem. Soc.* **2015**, *137*, 4908–4911. (e) Zhou, Z.; Liu, G.; Chen, Y.; Lu, X. Cascade Synthesis of 3-Alkylidene Dihydrobenzofuran Derivatives via Rhodium(III)-Catalyzed Redox-Neutral C–H Functionalization/Cyclization. *Org. Lett.* **2015**, *17*, 5874–5877. (f) Piou, T.; Rovis, T. Rhodium-Catalysed *syn*-Carboamination of Alkenes via a Transient Directing Group. *Nature* **2015**, *527*, 86–90. (g) Hu, Z.; Tong, X.; Liu, G. Rhodium(III) Catalyzed Carboamination of Alkenes Triggered by C–H Activation of *N*-Phenoxyacetamides under Redox-Neutral Conditions. *Org. Lett.* **2016**, *18*, 1702–1705. (h) Lerchen, A.; Knecht, T.; Daniliuc, C. G.; Glorius, F. Unnatural Amino Acid Synthesis Enabled by the Regioselective Cobalt(III)-Catalyzed Intermolecular Carboamination of Alkenes. *Angew. Chem. Int. Ed.* **2016**, *55*, 15166–15170. (i) Huang, X.; Liang, W.; Shi, Y.; You, J. Rh(III)-Catalyzed Chemoselective C–H Functionalizations of Tertiary Aniline *N*-oxides with Alkynes. *Chem. Commun.* **2016**, *52*, 6253–6256. (j) Wang, X.; Gensch, T.; Lerchen,

A.; Daniliuc, C. G.; Glorius, F. Cp*Rh(III)/Bicyclic Olefin Cocatalyzed C–H Bond Amidation by Intramolecular Amide Transfer. *J. Am. Chem. Soc.* **2017**, *139*, 6506–6512. (k) Pan, J.-L.; Xie, P.; Chen, C.; Hao, Y.; Liu, C.; Bai, H.-Y.; Ding, J.; Wang, L.-R.; Xia, Y.; Zhang, S.-Y. Rhodium(III)-Catalyzed Redox-Neutral Cascade [3 + 2] Annulation of *N*-Phenoxyacetamides with Propiolates via C–H Functionalization/Isomerization/Lactonization. *Org. Lett*. **2018**, *20*, 7131–7136. (l) Wu, Y.; Chen, Z.; Yang, Y.; Zhu, W.; Zhou, B. Rh(III)-Catalyzed Redox-Neutral Unsymmetrical C–H Alkylation and Amidation Reactions of *N*-Phenoxyacetamides. *J. Am. Chem. Soc.* **2018**, *140*, 42–45. (m) Yuan, W.-K.; Zhu, M.-H.; Geng, R.-S.; Ren, G.-Y.; Zhang, L.-B.; Wen, L.-R.; Li, M. Construction of Benzofuran-3(2*H*)-one Scaffolds with a Quaternary Center via Rh/Co Relay Catalyzed C–H Functionalization/Annulation of *N*-Aryloxyacetamides and Propiolic Acids. *Org. Lett*. **2019**, *21*, 1654–1658. (n) Wu, Y.; Pi, C.; Cui, X.; Wu, Y. Rh(III)-Catalyzed Tandem Acylmethylation/Nitroso Migration/Cyclization of *N*-Nitrosoanilines with Sulfoxonium Ylides in One Pot: Approach to 3-Nitrosoindoles. *Org. Lett*. **2020**, *22*, 361–364.

(6) (a) Wu, L.; Xu, H.; Gao, H.; Li, L.; Chen, W.; Zhou, Z.; Yi, W. Chiral Allylic Amine Synthesis Enabled by the Enantioselective $Cp^{X}Rh(III)$-Catalyzed Carboaminations of 1,3-Dienes. *ACS Catal.* **2021**, *11*, 2279−2287. (b) Ozols, K.; Onodera, S.; Woźniak, Ł.; Cramer, N. Cobalt(III)-Catalyzed Enantioselective Intermolecular Carboaminations via C−H Functionalizations. *Angew. Chem. Int. Ed.* **2021**, *60*, 655–659. (c) Duchemin, C.; Cramer, N. Enantioselective $Cp^{X}Rh^{III}$–Catalyzed Carboaminations of Acrylates. *Angew. Chem. Int. Ed.* **2020**, *59*, 14129–14133. (d) Piou, T.; Rovis, T. Rh(III)-Catalyzed Cyclopropanation Initiated by C−H Activation: Ligand Development Enables a Diastereoselective [2+1] Annulation of *N*-Enoxyphthalimides and Alkenes. *J. Am. Chem. Soc.* **2014**, *136*, 11292–11295. (e) Lerchen, A.; Knecht, T.; Daniliuc, C. G.; Glorius, F. Unnatural Amino Acid Synthesis Enabled by the Regioselective Cobalt(III)-Catalyzed

Intermolecular Carboamination of Alkenes. *Angew. Chem. Int. Ed.* **2016**, *55*, 15166–15170. (f) Liu, L.; Song, H.; Liu, Y.-H.; Wu, L.-S.; Shi, B.-F. Achiral $Cp^{X}Ir(III)$/Chiral Carboxylic Acid Catalyzed Enantioselective C–H Amidation of Ferrocenes under Mild Conditions. *ACS Catal.* **2020**, *10*, 7117–7122. (g) Farr, C. M. B.; Kazerouni, A. M.; Park, B.; Poff, C. D.; Won, J.; Sharp, K. R.; Baik, M.-H.; Blakey, S. B. Designing a Planar Chiral Rhodium Indenyl Catalyst for Regio- and Enantioselective Allylic C−H Amidation. *J. Am. Chem. Soc.* **2020**, *142*, 13996−14004.

(7) For examples on C−H functionalization/DG migration via Co catalysis, see: (a) Barsu, N.; Sen, M.; Premkumar, J. R.; Sundararaju, B. Cobalt(III) Catalyzed C-8 Selective C–H and C–O Coupling of Quinoline *N*-Oxide with Internal Alkynes via C–H Activation and Oxygen Atom Transfer. *Chem. Commun*. **2016**, *52*, 1338–1341. (b) Ikemoto, H.; Tanaka, R.; Sakata, K.; Kanai, M.; Yoshino, T.; Matsunaga, S. Stereoselective Synthesis of Tetrasubstituted Alkenes via a $Cp^{*}Co^{III}$-Catalyzed C−H Alkenylation/Directing Group Migration Sequence. *Angew. Chem. Int. Ed.* **2017**, *56*, 7156–7160. (c) Xu, X.; Zhang, L.; Zhao, H.; Pan, Y.; Li, J.; Luo, Z.; Han, J.; Xu, L.; Lei, M. Cobalt(III)-Catalyzed Regioselective C6 Olefination of 2-Pyridones Using Alkynes: Olefination/Directing Group Migration and Olefination. *Org. Lett.* **2021**, *23*, 4624–4629.

(8) For examples on C−H functionalization/DG migration via Ru catalysis, see: Li, M.; Yao, T.-Y.; Sun, S.-Z.; Yan, T.-X.; Wen, L.-R.; Zhang, L.-B. The Ruthenium(II)-Catalyzed C–H Olefination of Indoles with Alkynes: the Facile Construction of Tetrasubstituted Alkenes under Aqueous Conditions. *Org. Biomol. Chem.* **2020**, *18*, 3158–3163.

(9) For examples on C−H functionalization/DG migration via Mn catalysis, see: Zhou, X.; Li, Z.; Zhang, Z.; Lu, P.; Wang, Y. Preparation of Benzo[c]carbazol-6-amines via Manganese-Catalyzed Enaminylation of 1-(Pyrimidin-2-yl)-1*H*-indoles with Ketenimines and Subsequent Oxidative Cyclization. *Org. Lett*, **2018**, *20*, 1426–1429.

(10) For examples on C−H functionalization/DG migration via Rh catalysis, see: (a) Wu, X.; Lu, Y.; Qiao, J.; Dai, W.; Jia, X.; Ni, H.; Zhang, X.; Liu, H.; Zhao, F. Rhodium(III)-Catalyzed C–H Alkenylation/Directing Group Migration for the Regio- and Stereoselective Synthesis of Tetrasubstituted Alkenes. *Org. Lett.* **2020**, *22*, 9163–9168. (b) Zhao, F.; Gong, X.; Lu, Y.; Qiao, J.; Jia, X.; Ni, H.; Wu, X.; Zhang, X. Additive-Controlled Divergent Synthesis of Tetrasubstituted 1,3-Enynes and Alkynylated 3*H*-Pyrrolo[1,2-*a*]indol-3-ones via Rhodium Catalysis. *Org. Lett.* **2021**, *23*, 727–733. (c) Kumar, S.; Nunewar, S.; Usama, K. M.; Kanchupalli, V. Rh(III)-Catalyzed [3+2] Annulation and C−H Alkenylation of Indoles with 1,3-Diynes by C−H Activation. *Eur. J. Org. Chem*. **2021**, 2223–2229.

(11) For a review on C−H functionalization/DG migration, see: Wu, Y.; Pi, C.; Wu, Y.; Cui, X. Directing Group Migration Strategy in Transition-Metal-Catalysed Direct C–H Functionalization. *Chem. Soc. Rev.* **2021**, *50*, 3677–3689, and references cited therein.

(12) Only a handful examples of multi-step cascade processes triggered by C−H functionalization/DG migration have been discolosed to date, see: (a) Zhou, X.; Fan, Z.; Zhang, Z.; Lu, P.; Wang, Y. Construction of Pyrrolo[1,2-*a*]indoles via Cobalt(III)-Catalyzed Enaminylation of 1-(Pyrimidin-2-yl)-1*H*-indoles with Ketenimines and Subsequent Base-Promoted Cyclization. *Org. Lett*. **2016**, *18*, 4706–4709. (b) Chen, S.-Y.; Han, X.-L.; Wu, J.-Q.; Li, Q.; Chen, Y.; Wang, H. Manganese(I)-Catalyzed Regio- and Stereoselective 1,2-Diheteroarylation of Allenes: Combination of C−H Activation and Smiles Rearrangement. *Angew. Chem. Int. Ed*. **2017**, *56*, 9939–9943. (c) Wang, C.; Wang, A.; Rueping, M. Manganese-Catalyzed C−H Functionalizations: Hydroarylations and Alkenylations Involving an Unexpected Heteroaryl Shift. *Angew. Chem. Int. Ed*. **2017**, *56*, 9935–9938. (d) Zhu, C.; Kuniyil, R.; Jei, B. B.; Ackermann,

L. Domino C–H Activation/Directing Group Migration/Alkyne Annulation: Unique Selectivity by $d^6$-Cobalt(III) Catalysts. *ACS Catal.* **2020**, *10*, 4444–4450.

(13) (a) Zhou, J.; Shi, J.; Qi, Z.; Li, X.; Xu, H. E.; Yi, W. Mild and Efficient Ir(III)-Catalyzed Direct C–H Alkynylation of *N*-Phenoxyacetamides with Terminal Alkyne. *ACS Catal.* **2015**, *5*, 6999–7003. (b) Wu, X.; Wang, B.; Zhou, S.; Zhou, Y.; Liu, H. Ruthenium-Catalyzed Redox-Neutral [4 + 1] Annulation of Benzamides and Propargyl Alcohols via C–H Bond Activation. *ACS Catal.* **2017**, *7*, 2494–2499. (c) Wu, X.; Li, P.; Lu, Y.; Qiao, J.; Zhao, J.; Jia, X.; Ni, H.; Kong, L.; Zhang, X.; Zhao, F. Rhodium-Catalyzed Cascade Reactions of Indoles with 4-Hydroxy-2-Alkynoates for the Synthesis of Indole-Fused Polyheterocycles. *Adv. Synth. Catal.* **2020**, *362*, 2953–2960. (d) Zheng, G.; Zhou, Z.; Zhu, G.; Zhai, S.; Xu, H.; Duan, X.; Yi, W.; Li, X. Rhodium(III)-Catalyzed Enantio- and Diastereoselective C−H Cyclopropylation of *N*-Phenoxylsulfonamides: Combined Experimental and Computational Studies. *Angew. Chem. Int. Ed*. **2020**, *59*, 2890–2896.

(14) (a) Yi, W.; Chen, W.; Liu, F.-X.; Zhong, Y.; Wu, D.; Zhou, Z.; Gao, H. Rh(III)-Catalyzed and Solvent-Controlled Chemoselective Synthesis of Chalcone and Benzofuran Frameworks via Synergistic Dual Directing Groups Enabled Regioselective C–H Functionalization: A Combined Experimental and Computational Study. *ACS Catal*. **2018**, *8*, 9508−9519. (b) Bian, M.; Mawjuda, H.; Gao, H.; Xu, H.; Zhou, Z.; Yi, W. Lossen Rearrangement vs C–N Reductive Elimination Enabled by Rh(III)-Catalyzed C–H Activation/Selective Lactone Ring-Opening: Chemodivergent Synthesis of Quinolinones and Dihydroisoquinolinones. *Org. Lett.* **2020**, *22*, 9677–9682. (c) Yang, Y.; Zhang, K.; Yang, J.; Zhu, G.; Chen, W.; Zhang, C.; Zhou, Z.; Yi, W. Ru(II)-Catalyzed and Acidity-Controlled Tunable [5+1]/[5+2] Annulation for Building Ring-Fused Quinazolines and 1,3-Benzodiazepines. *Chem. Commun*. **2020**, *56*, 11315–11318. (d) Gao, H.; Lin, S.; Zhang, S.;

Chen, W.; Liu, X.; Yang, G.; Lerner, R. A.; Xu, H.; Zhou, Z.; Yi, W. gem-Difluoromethylene Alkyne-Enabled Diverse C−H Functionalization and Application to the on-DNA Synthesis of Difluorinated Isocoumarins. *Angew. Chem. Int. Ed*. **2021**, *60*, 1959–1966. (e) Zhao, F.; Qiao, J.; Lu, Y.; Zhang, X.; Dai, L.; Gong, X.; Mao, H.; Lu, S.; Wu, X.; Liu, S. Rh(III)-Catalyzed Divergent Synthesis of Alkynylated Imidazo[1,5-*a*]indoles and α,α-Difluoromethylene Tetrasubstituted Alkenes. *Org. Lett.* **2021**, *23*, 5766–5771.

(15) For a seminal reference on C–H activation of *N*-carbamoyl indoles, see: Schipper, D. J.; Hutchinson, M.; Fagnou, K. Rhodium(III)-Catalyzed Intermolecular Hydroarylation of Alkynes. *J. Am. Chem. Soc.* **2010**, *132*, 6910–6911.

(16) For a seminal reference on C–H activation assisted by the carbamoyl directing group, see: (a) Wang, D.-H.; Wasa, M.; Giri, R.; Yu, J.-Q. Pd(II)-Catalyzed Cross-Coupling of $sp^3$ C−H Bonds with $sp^2$ and $sp^3$ Boronic Acids Using Air as the Oxidant. *J. Am. Chem. Soc*. **2008**, *130*, 7190–7191. For a review on C–H activation assisted by the carbamoyl directing group, see: (b) Zhu, R.-Y.; Farmer, M. E.; Chen, Y.-Q.; Yu, J.-Q. A Simple and Versatile Amide Directing Group for C−H Functionalizations. *Angew. Chem. Int. Ed*. **2016**, *55*, 10578–10599.

(17) For a seminal reference on C–H activation with 4-hydroxy-2-alkynoates, see: Liao, G.; Song, H.; Yin, X.-S.; Shi, B.-F. Expeditious Synthesis of Pyrano[2,3,4-*de*]quinolines *via* Rh(III)-Catalyzed Cascade C–H Activation/Annulation/Lactonization of Quinolin-4-ol with Alkynes. *Chem. Commun*. **2017**, *53*, 7824–7827.

(18) For reviews on the synthesis of furan-2(5*H*)-ones, see: (a) Carter, N. B.; Nadany, A. E.; Sweeney, J. B. Recent Developments in the Synthesis of Furan-2(5*H*)-ones. *J. Chem. Soc*., *Perkin Trans. 1*, **2002**, 2324–2342. (b) Souza, M. V. N. D. The Furan-2(5*H*)-ones: Recent Synthetic Methodologies and Its Application in Total Synthesis of Natural Products. *Mini-Rev. Org. Chem*.

**2005**, *2*, 139−145. (c) Fedoseev, S. V.; Belikov, M. Y. Synthesis of 5-Hydroxyfuran-2(5*H*)-One Derivatives. *Chem. Heterocycl. Compd*. **2018**, *54*, 795−761.

(19) (a) Prasit, P.; Wang, Z.; Brideau, C.; Chan, C.-C.; Charleson, S.; Cromlish, W.; Ethier, D.; Evans, J. F.; Ford-Hutchinson, A. W.; Gauthier, J. Y.; Gordon, R.; Guay, J.; Gresser, M.; Kargman, S.; Kennedy, B.; Leblanc, Y.; Léger, S.; Mancini, J.; O'Neill, G. P.; Ouellet, M.; Percival, M. D.; Perrier, H.; Riendeau, D.; Rodger, I.; Tagari, P.; Thérien, M.; Vickers, P.; Wong, E.; Xu, L.-J.; Young, R. N.; Zamboni, R. The Discovery of Rofecoxib, [MK 966, VIOXX®, 4-(4′-Methylsulfonylphenyl)-3-phenyl-2(5*H*)-furanone], an Orally Active Cyclooxygenase-2 Inhibitor. *Bioorg. Med. Chem. Lett*. **1999**, *9*, 1773–1778. (b) Awad, A. A.; Sato, D.; Kusumoto, D.; Kamioka, H.; Takeuchi, Y.; Yoneyama, K. Characterization of Strigolactones, Germination Stimulants for the Root Parasitic Plants *Striga* and *Orobanche*, Produced by Maize, Millet and Sorghum. *Plant Growth Regul*. **2006**, *48*, 221–227. (c) Choudhury, A. R.; Mukherjee, S. Deconjugated Butenolide: a Versatile Building Block for Asymmetric Catalysis. *Chem. Soc. Rev.* **2020**, *49*, 6755–6788.

(20) For information on the screening of more additives in 1,4-dioxane, see entries 1-6 in Table S1 in Supporting Information.

(21) For information on the screening of more additives in acetone, see entries 7-12 in Table S1 in Supporting Information.

(22) Jiang, H.; Zhou, X. E.; Shi, J.; Zhou, Z.; Zhao, G.; Zhang, X.; Sun, Y.; Suino-Powell, K.; Ma, L.; Gao, H.; Yu, X.; Li, J.; Li, J.; Melcher, K.; Xu, H. E.; Yi, W. Identification and Structural Insight of an Effective PPARγ Modulator with Improved Therapeutic Index for Anti-diabetic Drug Discovery. *Chem. Sci*. **2020**, *11*, 2260–2268.

(23) (a) Kretschmer, C. B.; Nowakowska, J.; Wiebe, R. Solubility of Oxygen and Nitrogen in Organic Solvents from -25° to 50° C. *Ind. Eng. Chem.* **1946**, *38*, 506–509. (b) Achord, J. M.;

Hussey, C. L. Determination of Dissolved Oxygen in Nonaqueous Electrochemical Solvents. *Anal. Chem*. **1980**, *52*, 601–602. (c) Luehring, P.; Schumpe, A. Gas Solubilities (Hydrogen, Helium, Nitrogen, Carbon Monoxide, Oxygen, Argon, Carbon Dioxide) in Organic Liquids at 293.2 K. *J. Chem. Eng. Data*. **1989**, *34*, 250–252. (d) Franco, C.; Olmsted, J. Photochemical Determination of the Solubility of Oxygen in Various Media. *Talanta* **1990**, *37*, 905−909. (e) Quaranta, M.; Murkovic, M.; Klimant, I. A New Method to Measure Oxygen Solubility in Organic Solvents through Optical Oxygen Sensing. *Analyst* **2013**, *138*, 6243–6245. (f) Sato, T.; Hamada, Y.; Sumikawa, M.; Araki, S.; Yamamoto, H. Solubility of Oxygen in Organic Solvents and Calculation of the Hansen Solubility Parameters of Oxygen. *Ind. Eng. Chem. Res*. **2014**, *53*, 19331–19337.

(24) Sivaguru, J.; Solomon, M. R.; Poon, T.; Jockusch, S.; Bosio, S. G.; Adam, W.; Turro, N. J. The Reaction of Singlet Oxygen with Enecarbamates: A Mechanistic Playground for Investigating Chemoselectivity, Stereoselectivity, and Vibratioselectivity of Photooxidations. *Acc. Chem. Res*. **2008**, *41*, 387–400.

(25) (a) Yang, L.; Li, C.; Wang, D.; Liu, H. Cp*Rh(III)-Catalyzed C−H Bond Difluorovinylation of Indoles with α,α-Difluorovinyl Tosylate. *J. Org. Chem*. **2019**, *84*, 7320−7330. (b) Fei, X.; Li, C.; Yu, X.; Liu, H. Rh(III)-Catalyzed Hydroarylation of Alkyne MIDA Boronates via C−H Activation of Indole Derivatives. *J. Org. Chem*. **2019**, *84*, 6840−6850.

(26) (a) Hyster, T. K.; Rovis, T. Rhodium-Catalyzed Oxidative Cycloaddition of Benzamides and Alkynes via C−H/N−H Activation. *J. Am. Chem. Soc.* **2010**, *132*, 10565–10569. (b) Ackermann, L. Carboxylate-Assisted Transition-Metal-Catalyzed C−H Bond Functionalizations: Mechanism and Scope. *Chem. Rev.* **2011**, *111*, 1315–1345.

(27) (a) Satoh, T.; Miura, M. Oxidative Coupling of Aromatic Substrates with Alkynes and Alkenes under Rhodium Catalysis. *Chem. Eur. J.* **2010**, *16*, 11212–11222. (b) Gulías, M.; Mascareñas, J. L. Metal-Catalyzed Annulations through Activation and Cleavage of C−H Bonds. *Angew. Chem. Int. Ed*. **2016**, *55*, 11000−11019.

(28) For selected examples on oxidation by molecular oxygen in acetone, see: (a) Rathore, V.; Kumar, S. Visible-Light-Induced Metal and Reagent-Free Oxidative Coupling of $sp^2$ C–H Bonds with Organo-Dichalcogenides: Synthesis of 3-Organochalcogenyl Indoles. *Green Chem*. **2019**, *21*, 2670−2676. (b) Sankaralingam, M.; Lee, Y.-M.; Lu, X.; Vardhaman, A. K.; Nam, W.; Fukuzumi, S. Autocatalytic Dioxygen Activation to Produce An Iron(V)-Oxo Complex without Any Reductants. *Chem. Commun*. **2017**, *53*, 8348−8351. (c) Dong, J.; Lyu, X.; Wang, Z.; Wang, X.; Song, H.; Liu, Y.; Wang, Q. Visible-Light-Mediated Minisci C–H Alkylation of Heteroarenes with Unactivated Alkyl Halides Using $O_2$ as An Oxidant. *Chem. Sci*. **2019**, *10*, 976−982.

# Graphic Abstract